ASTROBIOLOGY
Volume 3, Number 4, 2003

Research Paper

Ozone Concentrations and Ultraviolet Fluxes on Earth-Like Planets Around Other Stars

ANTÍGONA SEGURA,[1] KARA KRELOVE,[1,*] JAMES F. KASTING,[1] DARRELL SOMMERLATT,[1] VICTORIA MEADOWS,[2] DAVID CRISP,[2] MARTIN COHEN,[3] and ELI MLAWER[4]

ABSTRACT

Coupled radiative–convective/photochemical modeling was performed for Earth-like planets orbiting different types of stars (the Sun as a G2V, an F2V, and a K2V star). O_2 concentrations between 1 and 10^{-5} times the present atmospheric level (PAL) were simulated. The results were used to calculate visible/near-IR and thermal-IR spectra, along with surface UV fluxes and relative dose rates for erythema and DNA damage. For the spectral resolution and sensitivity currently planned for the first generation of terrestrial planet detection and characterization missions, we find that O_2 should be observable remotely in the visible for atmospheres containing at least 10^{-2} PAL of O_2. O_3 should be visible in the thermal-IR for atmospheres containing at least 10^{-3} PAL of O_2. CH_4 is not expected to be observable in 1 PAL O_2 atmospheres like that of modern Earth, but it might be observable at thermal-IR wavelengths in "mid-Proterozoic-type" atmospheres containing $\sim 10^{-1}$ PAL of O_2. Thus, the simultaneous detection of both O_3 and CH_4—considered to be a reliable indication of life—is within the realm of possibility. High-O_2 planets orbiting K2V and F2V stars are both better protected from surface UV radiation than is modern Earth. For the F2V case the high intrinsic UV luminosity of the star is more than offset by the much thicker ozone layer. At O_2 levels below $\sim 10^{-2}$ PAL, planets around all three types of stars are subject to high surface UV fluxes, with the F2V planet exhibiting the most biologically dangerous radiation environment. Thus, while advanced life is theoretically possible on high-O_2 planets around F stars, it is not obvious that it would evolve as it did on Earth. Key Words: Terrestrial Planet Finder—Biomarkers—Ozone—Extrasolar planets. Astrobiology 3, 689–708.

INTRODUCTION

NASA's Planned Terrestrial Planet Finder (TPF) mission (Beichman *et al.*, 1999) and the European Space Agency's Darwin mission (Léger, 2000) are both designed to locate Earth-like planets around other stars and take spectra of their atmospheres and surfaces. The ultimate goal of these missions is to search for evidence of life by looking for various biomarker gases (Des

[1]Department of Geosciences, Pennsylvania State University, State College, Pennsylvania.
[2]NASA Jet Propulsion Laboratory/California Institute of Technology, Pasadena, California.
[3]Radio Astronomy Laboratory, University of California, Berkeley, California.
[4]Atmospheric and Environmental Research, Inc., Lexington, Massachusetts.
*Present address: Department of Planetary Sciences, Arizona State University, Tucson, Arizona.
Drs. Segura, Krelove, Kasting, Meadows, Crisp, and Cohen are NASA Astrobiology Institute members.

Marais *et al.*, 2002; Selsis *et al.*, 2002). Of these potential biomarker gases, the two most promising are O_2, which is produced almost entirely by photosynthesis on Earth, and ozone (O_3), which is produced photochemically from O_2. O_2 has a strong absorption band at 0.76 μm (Owen, 1980) that will fall within the observable spectral range of the planned optical/near-IR coronagraph version of TPF, and should be detectable for terrestrial planets with Earth-like atmospheres. O_3 has a strong 9.6-μm absorption band that should be detectable by an interferometric TPF or Darwin mission operating in the thermal IR (Léger *et al.*, 1993).

Ozone is a particularly sensitive indicator of photosynthetic life because of its nonlinear dependence on O_2 abundance (Ratner and Walker, 1972; Levine *et al.*, 1979; Kasting and Donahue, 1980; Kasting *et al.*, 1985; Schindler and Kasting, 2000). In particular, for the Earth, a 100-fold decrease in the atmospheric O_2 concentration from the present atmospheric level (PAL), to 10^{-2} PAL, reduces the total column depth of ozone by less than a factor of 3 (cf. Table 1 and Kasting *et al.*, 1985). Based on these previously generated photochemical model results, Schindler and Kasting (2000) found that the strength of the 9.6-μm band actually increases as O_2 decreases from 1 PAL down to 10^{-2} PAL. This result is suspect, however, because the stratospheric temperature profile was not calculated self-consistently in the Kasting *et al.* (1985) model. Instead, the current stratospheric temperature bulge, which peaks at 45 km in the modern atmosphere and is caused by absorption of UV radiation by ozone, was simply removed for O_2 concentrations of 10^{-1} PAL and below. This should lead to a slight overestimate in the ozone column depth at lower O_2 levels and a somewhat larger overestimate in the strength of the 9.6-μm band.

Here, we provide a more realistic model by coupling photochemical and radiative–convective calculations of stratospheric ozone and temperature at different O_2 levels. We also perform similar calculations for an Earth-like planet around sample main sequence F (HD 128167)- and K (HD 22049)-type dwarf stars, following Kasting *et al.* (1997). Our goal is to begin to build up a library of synthetic spectra of Earth-like planets for eventual use in interpreting TPF data. [As we generate and publish spectra, they will be made publicly available in digital form via the Virtual Planetary Laboratory public website (http://vpl.ipac.caltech.edu)]. At the same time, we calculate surface UV fluxes for different O_2 levels and use this information to speculate about the possibility of evolving complex life on planets around other stars.

MODEL DESCRIPTION

Photochemical/radiative–convective model

Our numerical model consists of a one-dimensional photochemical model (Pavlov and Kasting, 2002) that is loosely coupled to a one-dimensional, radiative–convective climate model (Pavlov *et al.*, 2000). Both programs use time-stepping algorithms to reach their solutions.

The radiative–convective model is actually a hybrid of two separate models. The time-stepping procedure and the solar (visible/near-IR) portion of the radiation code are from the model of Pavlov *et al.* (2000). The code incorporates a δ 2-stream scattering algorithm (Toon *et al.*, 1989) to calculate fluxes and uses four-term, correlated-*k* coefficients to parameterize absorption by O_3, CO_2, H_2O, O_2, and CH_4 in each of 38 spectral intervals (Kasting and Ackerman, 1986). At thermal IR wavelengths, we replaced the original algorithm of Pavlov *et al.* (2000) with the independent rapid radiative transfer model (RRTM) algorithm developed by Mlawer *et al.* (1997). This code calculates more accurate heating and cooling rates (and, hence, more reliable temperatures) in the stratosphere than did the original IR model. It uses 16-term sums in each of its spectral bands in which the *k*-coefficients are concentrated in the areas of most rapidly changing absorption, thereby providing better spectral resolution at altitudes where Doppler broadening is important. Spectral intervals and included absorber species are described in Mlawer *et al.* (1997), which fully details the method. A disadvantage of this version of the model is that the *k*-coefficients used therein are not applicable to dense, CO_2-rich atmospheres. This is not a problem for the current study because we have restricted our calculations to CO_2-poor atmospheres like that of the modern Earth. The most recent version of RRTM (http://rtweb.aer.com/) has been validated up to concentrations of 100 times current CO_2.

The RRTM code was fully coupled to the solar code, and the combination of the two routines was used to calculate temperature and tropospheric water profiles, as well as total radiative fluxes and heating and cooling rates. The (log pressure) grid extended from the assumed surface pressure of 1 bar down to 10^{-5} bar. This yielded slightly variable altitude ranges, with the top ranging from about 60 km at low O_2 to 70 km at 1 PAL of O_2. The program subdivided this range into 52 levels. Interpolation was required between the climate code and the photochemical code, which ran on a fixed altitude grid.

The photochemical model, originally developed by Kasting *et al.* (1985), is more fully detailed in Pavlov and Kasting (2002). It solves for 55 different chemical species that are linked by 217 separate reactions. The altitude range extended from 0 to 64 km in 1-km increments. Photolysis rates for various gas-phase species were calculated using a δ two-stream routine (Toon *et al.*, 1989) that accounts for multiple scattering by atmospheric gases and by sulfate aerosols. The model uses the reverse Euler method to time step to a solution.

Self-consistent climate/photochemical solutions were found by the following procedure: Starting from an initial guess for atmospheric composition and temperature, the photochemical model was used to generate converged vertical profiles for O_3 and stratospheric water vapor, along with other chemical species. These variables were introduced into the radiative–convective model, which was then used to calculate new vertical profiles for temperature and tropospheric water vapor. These were passed back to the photochemical model, and the whole procedure was repeated. Beginning from the solution for an adjacent (10 times higher or lower) oxygen level, about 10–20 complete iterations were required to generate stable, converged solutions. Convergence was somewhat slower at the lowest oxygen levels.

All simulations were performed with a constant ground pressure of 1 atm. The CO_2 mixing ratio was kept constant at 355 ppmv. Argon was maintained at 1% of the total atmospheric composition. N_2 was then allowed to vary to fill in the rest of the atmosphere, as oxygen was removed. Thus, PN_2 increases slightly at lower O_2 levels. As N_2 is mostly inert and does not absorb strongly in any of the relevant spectral regions, this small implied change should have little effect on our results. The photochemical model was run using a fixed solar zenith angle of 45°, as this was found to best reproduce the averaged 1976 U.S. Standard Atmosphere at 1 PAL of O_2. Calculated photolysis rates were multiplied by 0.5 to account for diurnal variation. The radiative–convective model used the daytime average solar zenith angle of 60° and the same factor of 0.5 for diurnal variation.

Producing a globally representative water profile in a one-dimensional model is difficult. For modern Earth the location of the tropopause cold trap at mid-latitudes is at an altitude of 8–10 km, while at the tropics it is 15–17 km, and it is there that stratospheric water levels are actually controlled. In order to produce a physically realistic water profile in our model, we calculated our tropospheric and stratospheric H_2O profiles independently. Temperature in the troposphere was assumed to follow a moist adiabat from ground level to the tropopause. Water vapor in this region was calculated in the climate code by assuming a Manabe–Wetherald (1967) relative humidity distribution. The relative humidity was further constrained such that it could not drop below 8%—the current relative humidity of Earth's cold trap. This was done to prevent stratospheric H_2O levels from dropping to essentially 0 at lower O_2 levels because of lower pressure and temperature at the calculated cold trap positions. Above the cold trap, water vapor was treated as a noncondensable gas, and its concentration was calculated by the photochemical code.

Clouds were not accounted for explicitly in these models. Instead, the surface albedo of the planet was adjusted so as to produce a surface temperature of 288 K for the present-Earth model (1 PAL of O_2). The resulting surface albedo, 0.20, is higher than the actual surface albedo, which is closer to 0.1. The surface albedo was then held constant in all other calculations. The resulting top-of-atmosphere (or planetary) albedo was ~0.21, which is lower than the actual value of ~0.31. Our simulated Earth thus receives slightly too much solar radiation because of its lower planetary albedo, but it also emits slightly too much IR radiation because it lacks the greenhouse effect of the clouds. By making this approximation, we effectively ignore any cloud feedback effects, along with any effect of clouds on the vertical temperature profile. As we assume a moist adiabatic lapse rate in the convective troposphere, the latter detail is of no great importance. For calculations on planets around other types of stars, we adjust the stellar fluxes to produce the same surface temperature (~288 K) under this same set of assumptions. So, we essentially moved the extrasolar "Earths" to the same exact position in their star's habitable zone.

Once the photochemical and climate model arrived at a converged solution, we introduced the resultant pressure and temperature profiles along with the mixing ratios of H_2O, O_3, CO_2, CH_4, and N_2O into a line-by-line radiative transfer program, the SMART (the Spectral Mapping Atmospheric Radiative Transfer) model. SMART was then used to calculate a high-resolution spectrum of the planet, as it would be seen from a vantage point above the atmosphere.

SMART radiative transfer model

To generate the synthetic planetary spectra, we used the SMART model (developed by D. Crisp and described in more detail in Meadows and Crisp, 1996). This model is a spectrum-resolving multiple-scattering model that incorporates the multilevel, multistream, discrete ordinate algorithm, DISORT (Stamnes *et al.*, 1988). DISORT provides solutions to the plane-parallel, monochromatic equation of radiative transfer, generating altitude- and angle-dependent radiances at each wavelength of interest for scattering, absorbing, and emitting atmospheres. Within SMART, the vertical inhomogeneity of realistic atmospheres is modeled with multiple atmospheric layers, and atmospheric optical properties (optical depth, single-scattering albedo, and the scattering phase function) are used to derive an accurate description of the solar and thermal radiation fields. SMART completely resolves the spectral variability associated with near-IR line absorption and UV predissociation and electronic bands of gases, as well as the wavelength dependence of the optical properties of airborne particles and the surface. (The only particles included in the current model are sulfate aerosols, and these are present in low enough concentrations that they have little effect on the calculated fluxes.)

We generated the high-resolution, angle-dependent solar radiance spectra through the following series of steps. First, the altitude-dependent temperature, pressure, and constituent abundances produced by the photochemical/radiative–convective model were used as input to SMART. Additional inputs included the UV and visible cross-sections, and temperature-dependent absorption coefficients for the atmospheric constituents, along with information on surface albedo, and basic planetary characteristics (e.g. radius, surface gravity, distance from the star, etc.). Surface albedos were specified at the lower boundary of the model, and stellar fluxes were specified at the top of the atmosphere at each spectral grid point. Based on the input data, SMART then employed a user-defined binning criterion to identify all monochromatic spectral segments within a broad spectral region that had similar optical properties at all points along the optical path. These segments were then mapped into a smaller number of quasimonochromatic bins. The equation of transfer was solved once for each bin, and the derived radiances were mapped back to their original wavelengths to create a high-resolution radiance spectrum. This mapping technique is used to significantly reduce the number of monochromatic multiple scattering calculations required to generate the spectrum, and rarely introduces radiance or heating rate errors larger than 1%.

The final suite of output radiance spectra was calculated for each user-specified solar zenith and azimuth angle, and number of streams. The "streams" are viewing angles, which are specified by an n-point Gaussian quadrature, where n is the number of streams. Four streams were adopted as the baseline for the calculations presented here (two up and two down) with corresponding upward stream viewing angles of 38° and 78° from the zenith. Unless otherwise specified, all spectra displayed in this paper are for a viewing angle of 38° from the zenith, and a solar zenith angle of 60°, looking down on the atmosphere from above. The disk-averaged spectrum of an extrasolar planet will depend on the geometry at which the observation is made. Numerical experiments are currently underway by our team, to assess the information content of disk-averaged spectra of Earth-like extrasolar planets observed from a range of viewing geometries. However, for the purposes of this paper, we provide these spectra at a specific viewing geometry, as illustrative examples of the type of spectra that may be observed.

To generate its spectra, SMART requires a spectrally resolved description of the atmospheric and surface optical properties that contribute to the absorption, emission, and scattering of radiation. For each gas, the wavelength-dependent monochromatic absorption coefficients for the IR rotation and vibration-rotation bands at each atmospheric level were derived with the line-by-line model, LBLABC (Meadows and Crisp, 1996), using the HITRAN 2000 absorption line database for all gases.

RESULTS

Past and present Earth models

Present Earth (1 PAL of O_2). The model was first tested by seeing how well it reproduces the current Earth's atmosphere. After making some semiempirical adjustments for handling water profiles, as described in the previous section, we were able to closely mimic the 1976 U.S. Standard Atmosphere temperature, O_3, and water profiles (Fig. 1). Although the isothermal layer (Fig. 1a) directly above the cold trap in the U.S. Standard Atmosphere does not appear in our profile, the shape is otherwise followed closely. Results are even better for the O_3 and water profiles, as can be seen in Fig. 1b and c. The total O_3 column depth in this atmosphere is 8.36×10^{18} cm^{-2}, or 0.311 atm-cm, which is close to the value of 0.32 atm-cm reported by McClatchey *et al.* (1971). (The U.S. Standard Atmosphere profile has a slightly larger column depth of 0.345 atm-cm.) Our calculated water vapor concentrations are within a factor of 2 of those in the U.S. Standard dry atmosphere at all altitudes.

The long-lived gases H_2, CH_4, N_2O, CO, and CH_3Cl were assigned fixed surface mixing ratios of 5.5×10^{-7}, 1.6×10^{-6}, 3×10^{-7}, 9×10^{-8}, and 5×10^{-10}, respectively, in this calculation. Given these mixing ratios, the model computed respective surface fluxes of -1.31×10^{12} g of H_2/year, 9.54×10^{14} g of CH_4/year, 1.32×10^{13} g of N_2O/year, 2.35×10^{15} g of CO/year, and 7.29×10^{12} g of CH_3Cl/year for the five gases. These fluxes (rather than the concentrations) were held fixed in the low-oxygen calculations described below. As these trace gases are all biogenic, this procedure is equivalent to assuming that the biota are unaffected by changes in atmospheric O_2 concentration or surface UV fluxes. We know that this cannot be true in reality; however, addressing this problem by treating the surface biota self-consistently is well beyond the scope of this paper. Fixed surface fluxes are better boundary conditions than fixed mixing ratios because the latter would imply changes in trace gas production rates that would have no link to physical reality.

Earth at lower O_2 levels. Several adjustments were made to the photochemical model in order to perform the calculations for O_2 contents ranging from 10^{-1} PAL to 10^{-5} PAL. As mentioned above, the surface fluxes of H_2, CH_4, N_2O, CO, and CH_3Cl were held constant at their (calculated) modern values. The sources of these gases are mostly biological. Their photochemical lifetimes change at lower O_2 levels; thus, their concentrations should change as well, provided that their sources remain constant. This, of course, is also an assumption, and it may not be accurate. Later, we describe one calculation in which the CH_4 flux was increased at lower O_2 levels to simulate increased recycling of organic matter by fermentation and methanogenesis.

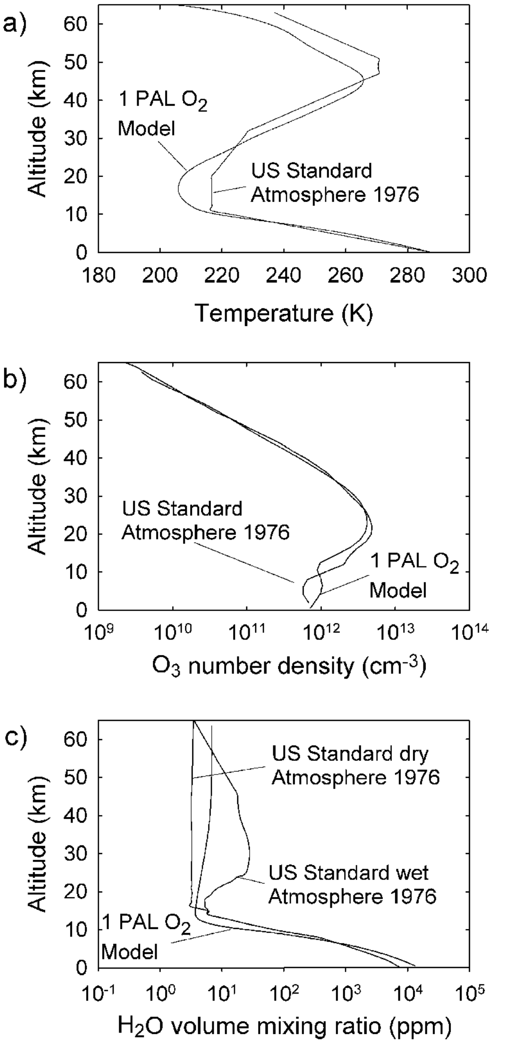

FIG. 1. Model results compared with vertical profiles from the 1976 U.S. Standard Atmosphere: (a) temperature, (b) O_3 number density, and (c) H_2O mixing ratios.

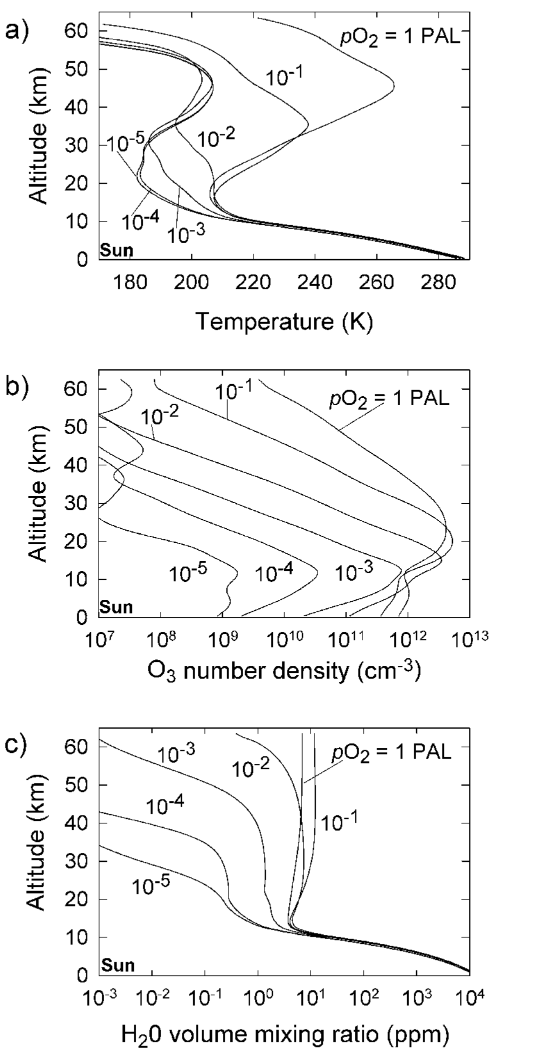

FIG. 2. Model results for Earth at different O_2 levels: (a) temperature, (b) O_3 number density, and (c) H_2O mixing ratios.

The results of these low-O_2 calculations are shown in Fig. 2. Overall, the variation in ozone concentrations with O_2 was close to that found in earlier calculations (Kasting and Donahue, 1980; Kasting *et al.*, 1985). The total ozone column depth decreased from 8.36×10^{18} cm^{-2} (0.311 atm-cm) at 1 PAL of O_2 to 2.24×10^{15} cm^{-2} (8.34×10^{-5} atm-cm) at 10^{-5} PAL of O_2 (see Table 1 and also Fig. 16). Meanwhile, the surface temperature dropped from 288 K to 285 K, mostly because of changes in planetary albedo. (O_3 absorbs sunlight at visible wavelengths in the troposphere. Thus, as its abundance drops, the planetary albedo increases by ~1%, thereby lowering the amount of absorbed sunlight and, thus, the surface temperature).

As expected, the temperature bulge in the middle stratosphere decreased in amplitude as the O_2 concentration decreased from 1 PAL to 10^{-2} PAL (Fig. 2a). Below 10^{-2} PAL of O_2, upper stratospheric temperatures remained nearly constant, but the temperature near the tropopause continued to decrease. As O_2 was removed, the ozone layer moved downward (Fig. 2b) and became thinner, although the total column depth did not decrease significantly until PO_2 dropped below 10^{-2} PAL (Table 1). The amount of stratospheric water (Fig. 2c) increased as O_2 decreased from 1 PAL to 10^{-1} PAL. This resulted from a slight warming of the tropopause cold trap. Below 10^{-1} PAL of O_2, stratospheric water vapor decreased sharply as a consequence of increased photolysis associated with lack of UV shielding by O_2 and O_3. Note that oxidation of CH_4 cannot maintain high stratospheric H_2O mixing ratios because CH_4 is itself disappearing as O_2 levels become lower (see Fig. 3a).

One curious feature of the temperature profiles that deserves explanation is the high (48-km) stratospheric temperature bulge that develops at low O_2 levels. This bulge is caused by absorption of solar near-IR radiation by CO_2. We should note that our radiative model, which was designed for the present atmosphere, treats these CO_2 bands rather crudely using four-term *k*-coefficients, so the accuracy of our stratospheric temperatures at low O_2 levels is probably not very good. Because the anomalous temperature bulge occurs so high, however, it should have little effect on either our calculated O_3 column depths or on our simulated spectra.

CH_4 and N_2O are both considered important secondary biomarkers, so it is instructive to see how their concentrations vary as a function of O_2 level. Figure 3 shows CH_4 and N_2O profiles calculated under the assumption of constant upward surface flux. The N_2O mixing ratio de-

TABLE 1. OZONE COLUMN DEPTH FOR PLANETS WITH DIFFFERENT O_2 LEVELS AND AROUND DIFFERENT STARS

	O_3 *column depth* (*cm*$^{-2}$)		
O_2 *level (PAL)*	*Sun*	*K2V*	*F2V*
10^0	8.36×10^{18}	6.64×10^{18}	1.56×10^{19}
10^{-1}	7.16×10^{18}	4.73×10^{18}	1.43×10^{19}
10^{-2}	3.33×10^{18}	2.09×10^{18}	9.11×10^{18}
10^{-3}	6.79×10^{17}	2.87×10^{17}	2.19×10^{18}
10^{-4}	3.26×10^{16}	3.94×10^{16}	2.27×10^{16}
10^{-5}	2.24×10^{15}	4.27×10^{15}	3.02×10^{15}

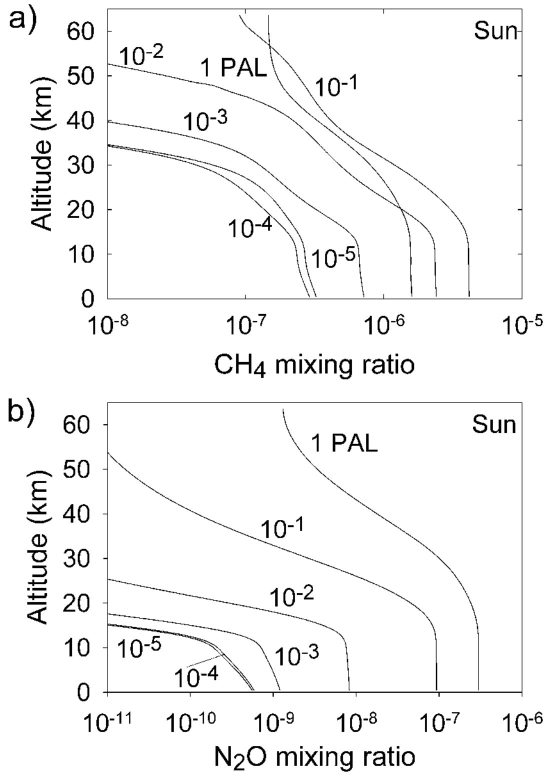

FIG. 3. Vertical mixing ratios of other biogenic gases for the cases shown in Fig. 2 considering a constant upward surface flux: (a) CH_4 and (b) N_2O.

creases dramatically at lower O_2 levels (Fig. 3b), in agreement with previous calculations (Kasting and Donahue, 1980). The N_2O decrease occurs because of decreased shielding of solar UV radiation by O_3. CH_4 exhibits a more complex behavior, again in accord with earlier calculations (Kasting and Donahue, 1980). The surface CH_4 concentration increases as PO_2 drops from 1 PAL to 0.1 PAL, then decreases as PO_2 decreases further. The increase in CH_4 at 0.1 PAL of O_2 is caused by decreased tropospheric O_3 concentrations (Fig. 2b) and correspondingly lower tropospheric OH concentrations. Reaction with OH is the main sink for CH_4 in the modern atmosphere. At O_2 levels below 0.1 PAL, increased rates of tropospheric H_2O photolysis (caused by decreases in UV shielding by ozone) result in lower surface concentrations of CH_4 and other reduced gases (Fig. 4).

We note parenthetically that current TPF plans call for a spectral resolution that is sufficiently low that these trace species will only be unambiguously detectable under ideal circumstances. The simultaneous presence of reduced gases such as CH_4 and N_2O along with O_2 (or O_3) is considered to be the most reliable spectroscopic signature of life (Lovelock, 1965; Sagan *et al.*, 1993; Des Marais *et al.*, 2002).

A signature that would be detectable by TPF is the 9.6-μm absorption band of ozone. Ozone could be detected for O_2 levels from 1 down to $\sim 10^{-3}$ PAL (Fig. 5). These results are similar to those found by Schindler and Kasting (2000) except that the 9.6-μm band is not quite as deep at 0.1 PAL of O_2 because our stratosphere is still relatively warm at this O_2 level. Recall that Schindler and Kasting (2000) assumed an isothermal stratosphere for all O_2 levels <1 PAL.

A low-O_2/high-CH_4 case: the Mid-Proterozoic Earth. Actual atmospheric CH_4 concentrations at low O_2 levels may have been even higher than shown in Figs. 3 and 4. Several authors have proposed that PO_2 was significantly lower than today (but still well above zero concentration) during the Mid-Proterozoic Era between 2.3 Ga and ~0.8 Ga (Canfield, 1998; Canfield *et al.*, 2000; Anbar and Knoll, 2002). ("Ga" stands for "giga-annum" or "billions of years ago.") We take $PO_2 = 0.1$ PAL as a reasonable estimate for this time period. Recently, Pavlov *et al.* (2003) suggested that these lower O_2 levels may have been accompanied by significantly higher concentrations of methane. Today, most of the organic matter produced by marine photosynthesis is recycled either by aerobic oxidation or by bacterial sulfate reduction in sediments. In a low-O_2/low-sulfate Mid-Proterozoic ocean much of this organic matter may have been recycled by fermentation and methanogenesis. CH_4 fluxes of 10–20 times the present biological flux are possible (Pavlov *et al.*, 2003).

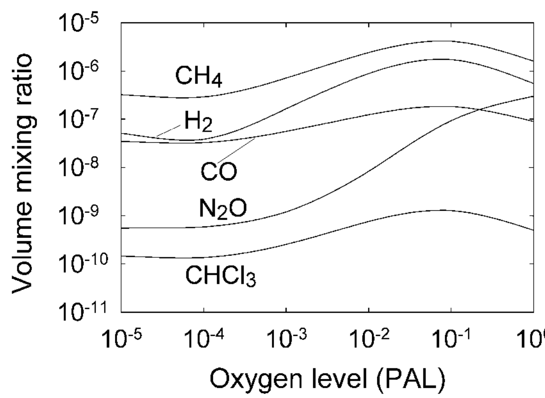

FIG. 4. Surface mixing ratios of biogenic trace gases for the cases shown in Fig. 2.

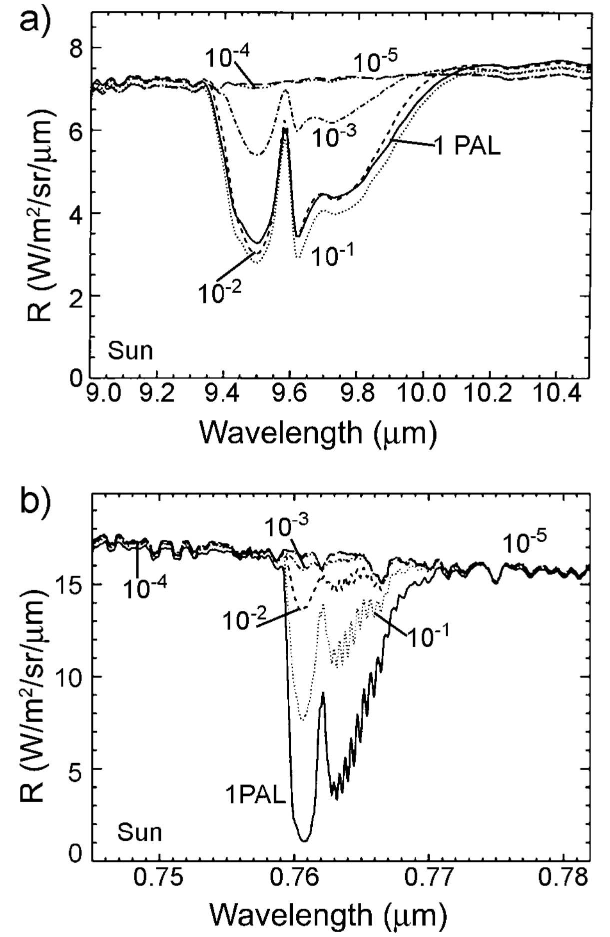

FIG. 5. Spectra calculated by the SMART model for the cases shown in Fig. 2: (a) O_3 9.6-μm band and (b) O_2 0.76-μm band.

The atmospheric CH_4 concentrations accompanying such high surface CH_4 fluxes are even higher than one might expect because the photochemical lifetime of CH_4 increases as its concentration increases. The reason is that OH is the sink for CH_4, but CH_4 is also the primary sink for OH. Pavlov *et al.* (2003) found that the atmospheric CH_4 concentration increases almost quadratically with surface CH_4 flux. In our model the (calculated) present CH_4 flux of 9.54×10^{14} g/year produced a surface CH_4 concentration of 4.15 ppm at $PO_2 = 0.1$ PAL. Our calculated methane flux is about 80% larger than the best estimate for the modern methane flux, 5.35×10^{14} g/year (Houghton *et al.*, 1994), indicating that we are underestimating the atmospheric lifetime of CH_4 in our model. The discrepancy is caused at least partly by our low assumed solar zenith angle of 45°, which is 15° lower than the sunlit hemispheric average. The identical error is made at all O_2 levels, however, so it should not affect the relative amount of CH_4 in these atmospheres compared with the present atmosphere. We have also done model simulations for surface CH_4 mixing ratios of 20 ppm and 100 ppm (Fig. 6a). These concentrations corresponded to surface CH_4 fluxes of 2.7×10^{15} g year^{-1} and 7.9×10^{15} g year^{-1}, respectively. These fluxes are about five and 15 times larger than the present CH_4 flux, which is within the range of values predicted for the Mid-Proterozoic. The temperature profile used for these runs was the one obtained for the 4.15 ppm CH_4 case. Our climate model actually predicted lower surface temperatures (i.e., an anti-greenhouse effect)

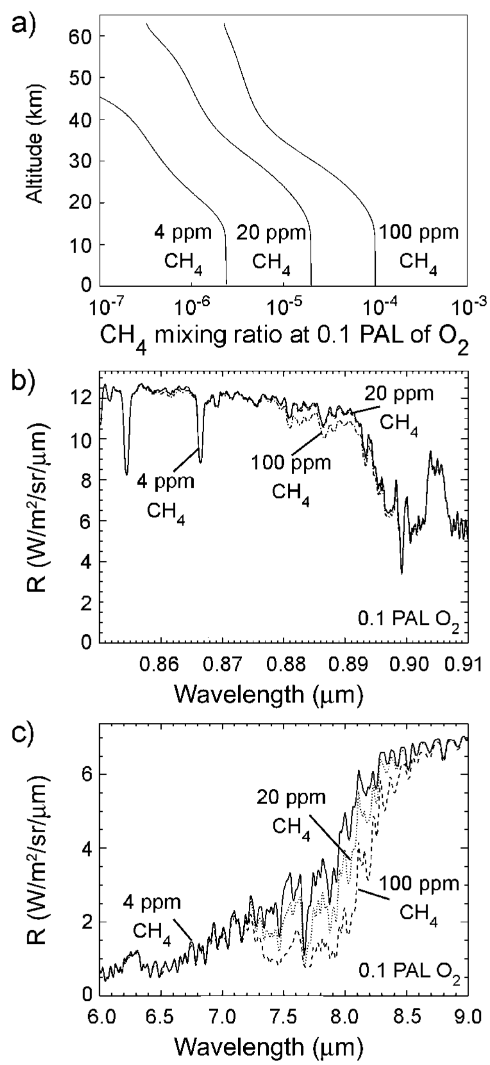

FIG. 6. Profiles and spectra for a "mid-Proterozoic-type" atmosphere containing 0.1 PAL of O_2 and various amounts of CH_4: (a) CH_4 profiles, (b) visible/near-IR spectra showing the CH_4 bands, and (c) thermal-IR spectra showing the CH_4 7.7-μm band.

for these high CH_4 levels, but we are not sure whether this is a reliable result or simply an artifact of the limited range of our infrared *k*-coefficients. We will investigate this issue more thoroughly elsewhere. In any case, this issue has little bearing on the results presented below.

Calculated CH_4 vertical profiles and spectra for these high-CH_4/low-O_2 models are shown in Fig. 6. Both O_2 and O_3 would be easily detectable in such a planetary atmosphere (Fig. 5). The CH_4 absorption band at 7.7 μm could conceivably be detectable as well by an IR interferometer in the 100 ppm CH_4 case (Fig. 6c). Thus, Mid-Proterozoic type atmospheres might exhibit a detectable, nearly unambiguous signal of extraterrestrial life. The potential for making such an observation had not been previously suggested for a first-generation TPF instrument. In the visible/near-IR, the CH_4 bands are weaker (Fig. 6b), so it is less likely that one could obtain such an interesting result.

Earth-like planets around other stars

From missions such as TPF or Darwin we hope to obtain spectral information about Earth-like planets around other stars. The ones with the greatest potential to be habitable appear to be planets around the F, G, and early K-type stars (Kasting *et al.*, 1993). Stars earlier than F0 have very short (<2 Gyr) main sequence lifetimes and, hence, have a low probability of harboring planets with complex life. Their habitable zones migrate outwards rapidly, so even microbial life might not have time to develop in these systems. Planets orbiting stars later than ~K5 are likely to become tidally locked, which may be a problem for habitability (although see discussion below). We looked at an F2V star and a K2V star to see how an Earth-like planet might differ from a planet circling our Sun.

Preparation of the stellar spectra

The sample stars used were HD 128167, an F2V star about 12 pc distant from Earth, and HD 22049, a K2V star only 3.2 pc distant. Kasting *et al.* (1997) originally chose these stars for their study because their UV spectra had been observed by the International Ultraviolet Explorer (IUE) satellite. We used the same stars so that we could compare with their earlier results.

HD 128167, σ Bootis, is an average, middle-aged F-type dwarf, ~2 Ga old (Habing *et al.*, 2001), with an effective temperature of 6,700 K (Habing *et al.*, 2001) and a metallicity slightly below solar standard (Cayrel de Strobel *et al.*, 1992). It has been reported by Habing *et al.* (2001) to exhibit excess IR emission, which suggests the presence of an Oort Cloud-like structure at perhaps 100–200 AU. This excess emission, however, occurs well longward of 0.320 μm, the point at which our IUE spectra end.

HD 22049, ε Eridani, is a young K-type dwarf. Its age is estimated at only ~0.5 Ga (Habing *et al.*, 2001), setting this star within the time frame of the heavy bombardment in our own inner Solar System. ε Eridani is known to have a dust ring and is host to a "warm Jupiter," a planet of about 1 Jupiter mass orbiting at 3.4 AU (Cumming *et al.*, 1999). It is chromospherically active, so it has relatively more UV flux than an older K star. While these characteristics make ε Eridani a less than ideal candidate for the title of "average K-type dwarf," they also mean that IUE measurements of ε Eridani are both more frequent and more reliable than observations of less active K dwarfs.

Kasting *et al.* (1997) had already obtained UV spectra for these same two stars from the IUE database. New observations have been added to the database since that time, however, so we repeated this process. We also used a realistic visible/IR spectrum for each star, as compared with the blackbody curves previously used by Kasting *et al.* (1997). Massa *et al.* (1998) have quantified the problems in the absolute calibration of the IUE Final Archive of low-resolution spectra, finding up to 40% errors at short shortwave (SW) wavelengths and 10–15% problems at long SW and all longwave (LW) wavelengths. However, Massa and Fitzpatrick (2000) have developed software that correctly reprocesses and absolutely recalibrates these spectra, and have verified the results as correct at the ~3% level. We have implemented these correction routines and applied them to the IUE spectra in this paper.

The F star spectrum, which exhibited relatively high UV fluxes, was prepared as follows: A composite spectrum was created by matching the coadds of seven SW and four LW observed IUE spectra from 115 nm to 335 nm to an unreddened Kurucz synthetic spectrum (Kurucz, 1979; Buser and Kurucz, 1992) for an effective temperature of 6,733 K, log surface gravity of 4.33, with solar abundances. From 290 nm to ~160 μm, the spectrum is purely photospheric, and the region between 290 nm and 335 nm was used to merge the empirical UV spectrum with the photosphere.

Secondary LW camera data between 195 nm and 230 nm and mixed secondary LW camera and primary camera data longward of 230 nm were combined into a patch between the two datasets. The patched data were then shifted slightly downward so as to match the SW data at 195 nm and the Kurucz model at 320 nm.

The K star spectrum was based on the results of coadding 65 SW and 19 LW corrected, recalibrated IUE spectra from 115 nm to 335 nm. The resulting IUE spectra, corrected by Massa for the Astrophysics Data Facility, can be viewed on the websites mariecurie.gsfc.nasa.gov/iue/temp/sw_lo_105.html and mariecurie.gsfc.nasa.gov/iue/temp/lw_lo_080.html. However, to derive the numerical data, the reprocessing must be applied to all 84 valid IUE spectra, and the results are coadded appropriately as we have done. The coadded IUE spectrum was merged with an unreddened Kurucz photosphere (for 5,180 K, 4.75, −0.09), scaled absolutely to match 14 optical, near- and mid-IR broadband photometric points using the method described by Cohen *et al.* (2003). In the region from 355 to 751 nm, we substituted the average of two independent spectra observed by Burnashev (1985), rescaling the average by a factor of 1.07. Thus, the region from 115 to 751 μm is based entirely on observations of HD 22049 itself. Only beyond do we use a model to extrapolate the energy distribution.

The procedure outlined so far determines the shape of the stellar spectrum and intensity of these stellar spectra as seen from the Earth, but not their intensities as felt by orbiting planets. Absolute fluxes were determined by normalizing the entire curve to the total observed stellar flux, as calculated from the distance and effective temperature of the star. The composite stellar spectra were then renormalized so as to be appropriate for a planet at the same relative position within their star's habitable zone as the position of the Earth around our Sun. The normalized spectra take into account the different planetary albedos for Earth under different wavelengths of incident radiation. The total flux from the Sun calculated from its spectrum was 1,375 W/m^2. The corresponding normalized flux for the F2V star was 1,375 × (1.11) = 1,526 W/m^2, while the flux for the K2V star was 1,375 × (0.95) = 1,306 W/m^2. The normalization constants, 1.11 and 0.95, are from Kasting *et al.* (1993) and Kasting *et al.* (1997). Figure 7 shows comparative spectra for the three stars. Calculating planetary distances ($r = 1$ AU $[(L/L_{sun})/(Flux/Flux_{sun})]^{1/2}$) puts the F2V planet at 1.69 AU and the K2V planet at 0.53 AU from their parent stars.

The possible effect of enhanced chromospheric activity on a star's emitted UV flux was estimated by looking at two active G0V stars observed by IUE: HD 114710 (low activity) and HD 206860 (high activity). A planet in the habitable zone of these stars would receive ~2.5 times more UV radiation than Earth in the range from 176 nm to 250 nm. This suggests that an older, quieter K2V dwarf star might receive 2.5 times less UV radiation than our hypothetical planet around ε Eridani. These conclusions are based on using the identical method of merging appropriate, unreddened, and absolute Kurucz photospheric spectra (6,008 K, 4.44, 0.10 for HD 114710; 5,885 K, 4.40, −0.09 for HD 206860) with corrected and recalibrated, coadded (HD 114710, three SW, four LW spectra; HD 206860, 11 SW, seven LW) IUE spectra to the G0V stars.

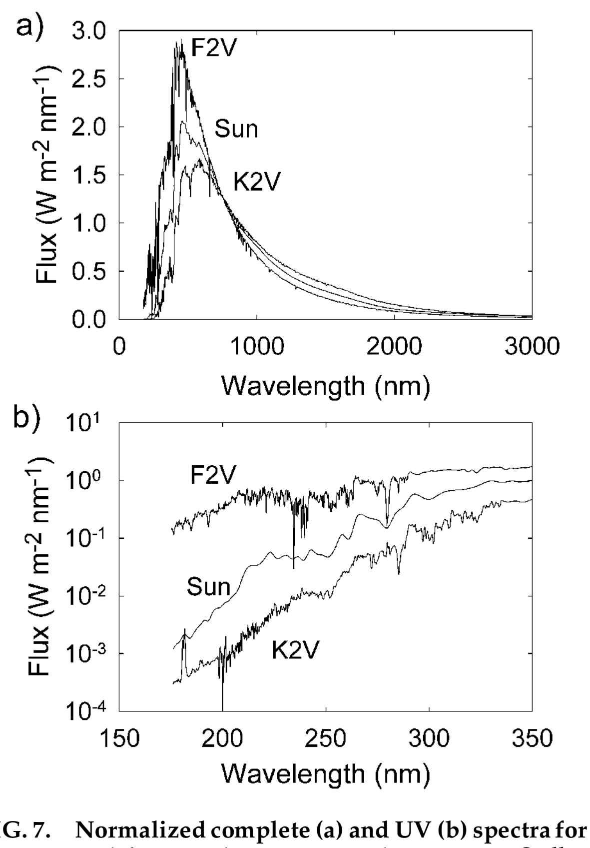

FIG. 7. Normalized complete (a) and UV (b) spectra for the Sun and for our chosen F2V and K2V stars. Stellar fluxes were normalized in such a way as to produce a surface temperature of 288 K for an Earth-like planet with 1 PAL of O_2 in its atmosphere.

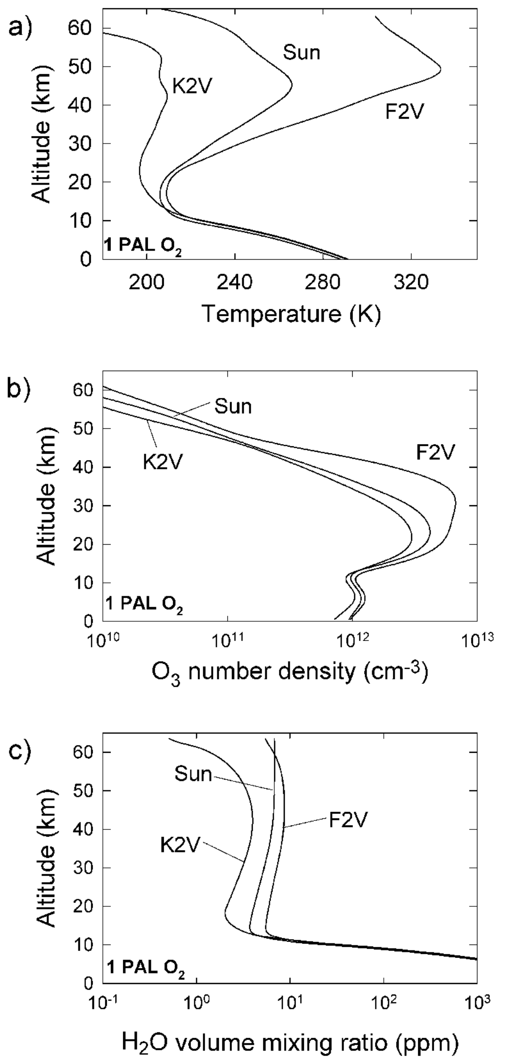

FIG. 8. Model results for a planet with a 1 PAL O_2 atmosphere circling different types of stars: (a) temperature, (b) ozone number densities, and (c) H_2O mixing ratios.

Comparisons at 1 PAL of O_2. We began our simulations of planets around other stars by performing calculations for a 1 PAL O_2 atmosphere. The resulting vertical profiles of temperature, O_3, and H_2O are shown in Fig. 8, along with the previously calculated results for modern Earth.

The calculated temperature profiles look much as expected (Fig. 8a). Up to ~12 km, there is very little difference among the F, G, and K star results. (This is because of how we normalized the stellar fluxes. We actually performed one additional, small normalization step at this point to force the calculated surface temperatures to be 288 K for the 1 PAL O_2 models.) Stratospheric temperatures are quite different, however, with the K2V stratosphere being the coolest, while the F2V stratosphere is the by far the warmest. The warm stratosphere on the F2V planet is a consequence of the much higher stellar UV flux and the correspondingly greater absorption of UV energy by ozone. For ozone, the solar and K2V profiles are similar, while the F2V planet has a significantly higher abundance (Fig. 8b). However, the F2V ozone layer is not as thick as in the Kasting *et al*. (1997) study in which stratospheric temperatures were held constant.

Figure 9 shows simulated 9.6-μm O_3 bands (Fig. 9a) and 15-μm CO_2 bands (Fig. 9b) for these 1 PAL O_2 atmospheres. The CO_2 band shows clearly the influence of stratospheric temperature: It is deepest for the (cold stratosphere) K2V planet and shallowest for the (warm stratosphere) F2V planet. Because the band is being seen in absorption, the temperature contrast between the cool stratosphere and the warm lower troposphere and surface determines the relative depth of the band. The O_3 band behaves somewhat dif-

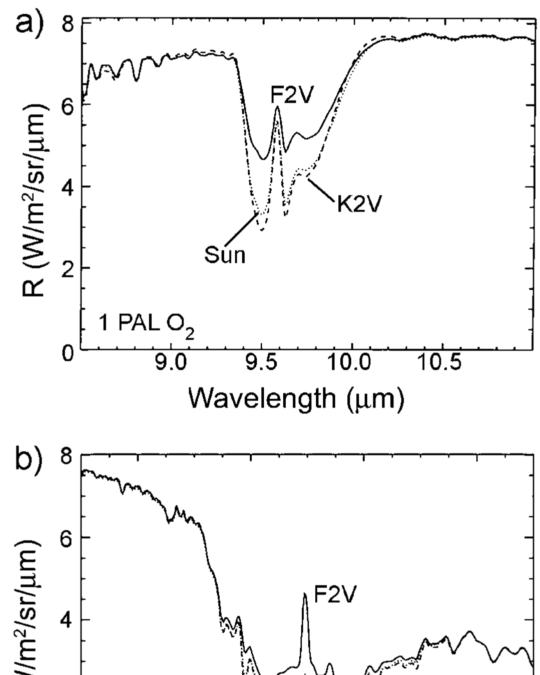

FIG. 9. Thermal-IR spectra of the three atmospheres shown in Fig. 8 in the vicinity of the O_3 9.6-μm band (a) and the CO_2 15-μm band (b).

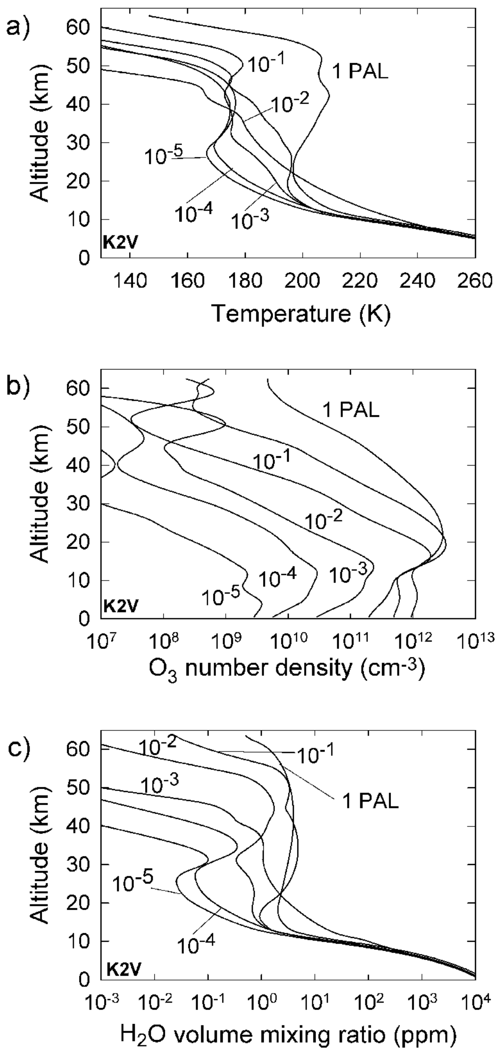

FIG. 10. Model results for an Earth-like planet circling a K2V star at different O_2 levels: (a) temperature, (b) O_3 number density, and (c) H_2O mixing ratios.

ferently because both O_3 concentration and temperature vary from planet to planet. The O_3 band has nearly the same strength for the K2V and solar cases but is significantly shallower in the F2V case. This would have been difficult to predict without actually doing the calculation.

Results for lower O_2 levels. The results of coupled photochemical/climate modeling for the Earth-like planets with lower O_2 levels are shown in Figs. 10 and 11 for the K2V and F2V stars, respectively. Surface trace gas mixing ratios for the planets around the two stars are shown in Fig. 12. Figures 13 and 14 show the calculated planetary spectra in the vicinity of the 9.6-μm O_3 band and the oxygen band at 0.76 μm for K2V and F2V planets, respectively. For the planet around the K2V star (Fig. 13a), the dependence of the 9.6-μm band strength on PO_2 is similar to the solar case (Fig. 5a). The band remains nearly the same strength down to PO_2 = 0.01 PAL and then begins to disappear below that level. For the F2V case, though, the results are quite different. The 9.6-μm band is shallow at 1 PAL of O_2 (because of the high stratospheric temperatures) and then deepens considerably as the O_2 level drops to 10^{-2} PAL. The total band strength for the 10^{-3} PAL case is nearly the same as for the 1 PAL case, although the details of the band shape are different. This suggests that a low-resolution TPF instrument would have a hard time distinguishing between 10^{-3} PAL of O_2 and 1 PAL of O_2 on a planet around an F2V star.

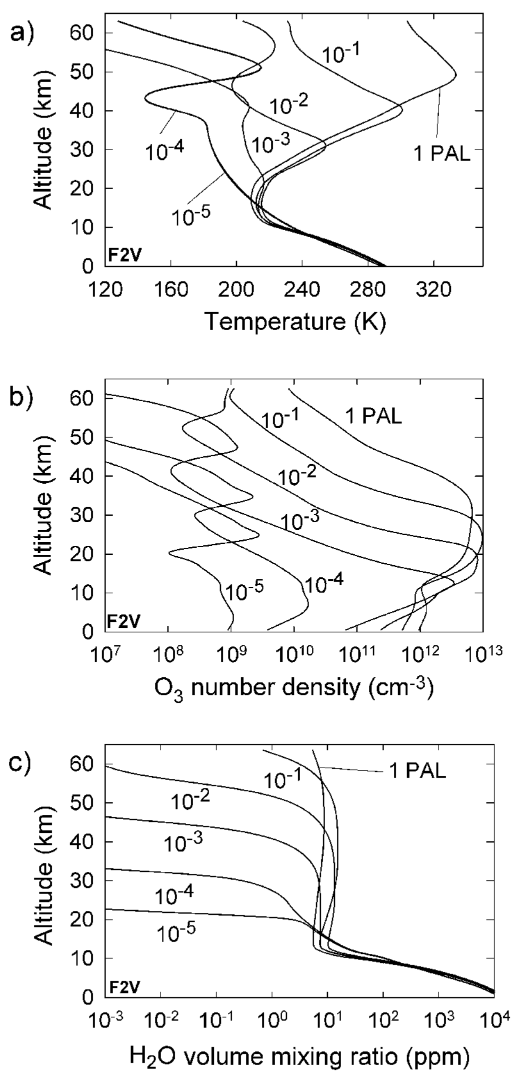

FIG. 11. Model results for an Earth-like planet circling a F2V star at different O_2 levels: (a) temperature, (b) O_3 number density, and (c) H_2O mixing ratios.

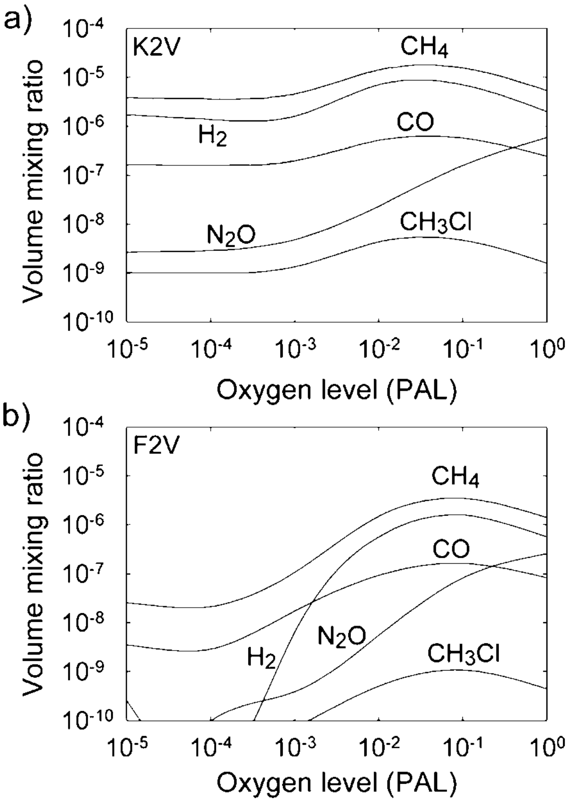

FIG. 12. Surface concentrations of biogenic trace gases for the cases shown in Figs. 10 and 11: (a) K2V star and (b) F2V star.

The behavior of the biogenic trace gases is also qualitatively different for the K- and F-star planets (Fig. 12) than for the Earth around our Sun (Fig. 5). CH_4 and N_2O levels are systematically higher for the K2V planet and lower for the F2V planet because of the difference in stellar UV fluxes. Note that trace gas concentrations are different from Earth at *all* O_2 levels (including 1 PAL) because we have assumed the same surface fluxes as for modern Earth (see above). At 0.1 PAL of O_2, the CH_4 concentration for the K2V planet is already of the order of 20 ppm, even without assuming a higher surface flux. This suggests that the simultaneous detection of CH_4 and O_2 on planets around K stars is within the realm of feasibility.

Surface UV fluxes on Earth-like planets around other stars

In addition to their possible use in interpreting future TPF data, the calculations described here can be used to examine the surface radiation environment on Earth-like extrasolar planets. The surface flux of UV radiation is of great concern to scientists (and non-scientists) today because of its ability to damage the cells and even the DNA of modern organisms. Most current research is concerned with damage by radiation in the range of 280–315 nm (known as UV-B) and 315–400 nm (UV-A). At present, little or no radiation shortward of 280 nm (UV-C) penetrates the atmosphere. However, without our relatively thick O_3 layer, this highly damaging radiation would also penetrate to ground level.

As mentioned earlier, comparative calculations at 1 PAL of O_2 were done previously by Kasting *et al.* (1997) except that the stratospheric temperatures were not computed self-consistently. Kasting *et al.* (1997) found that both the K2V and F2V planets actually received less surface UV radiation than does Earth. We find that the K2V planet receives about 0.4 times the radiation than does Earth in the range from 200 to 400 nm, while the F2V planet receives 1.6 times more radiation than

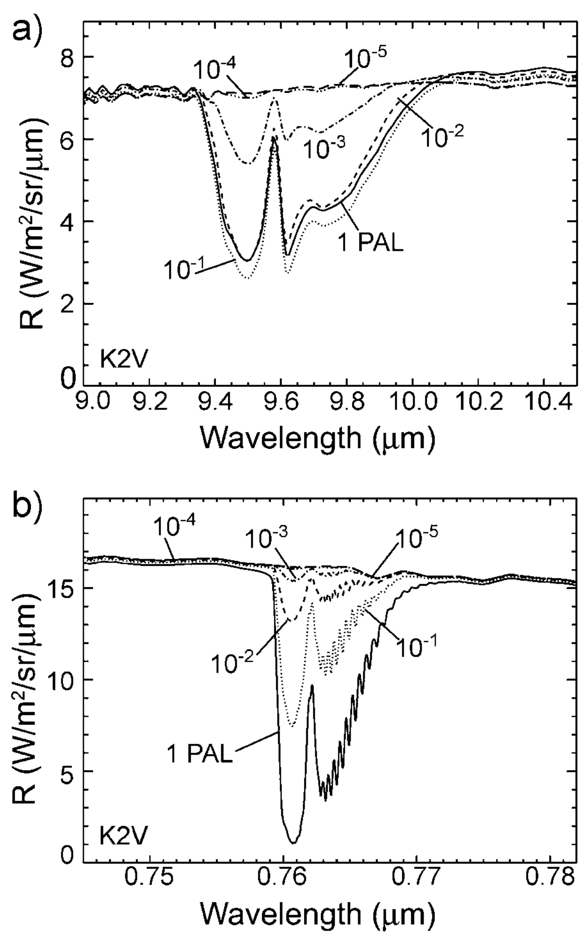

FIG. 13. O_2 and O_3 bands for the K2V planet (see Fig. 10): (a) O_3 9.6-μm band and (b) O_2 0.76-μm band.

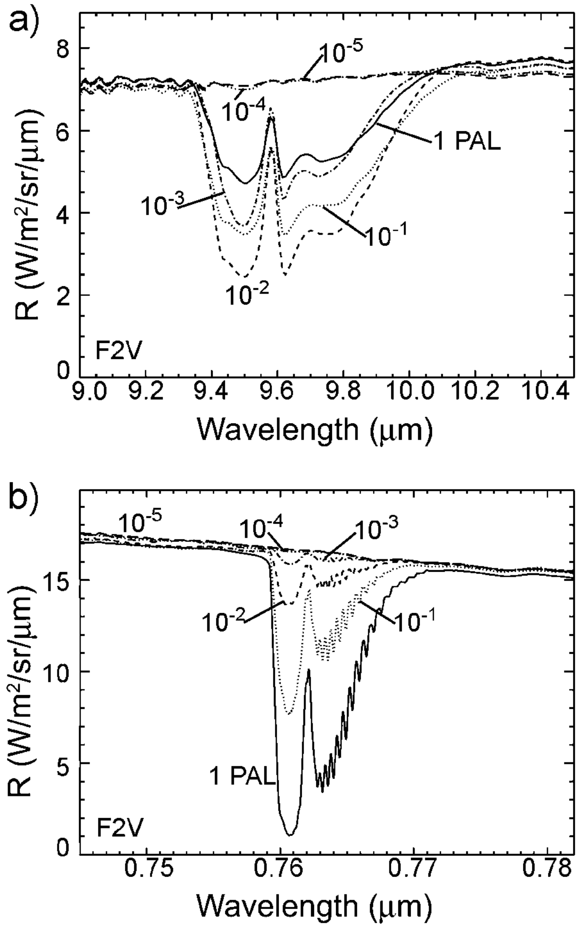

FIG. 14. O_2 and O_3 bands for the F2V planet (see Fig. 11): (a) O_3 9.6-μm band and (b) O_2 0.76-μm band.

does Earth (Table 2 and Fig. 15). In the dangerous UV-B wavelength range, the K2V planet again receives about 0.4 times Earth's flux, but the F2V planet receives only 0.85 times Earth's flux, meaning that one is better protected there than on Earth. These results are not surprising given the significantly higher O_3 column depth for the F2V planet (Fig. 16 and Table 1). The additional O_3 formed in this case more than makes up for the additional UV-B radiation from the F2V star.

The story is quite different, though, at lower O_2 levels. Figure 16 shows ozone column depth as a function of O_2 level for planets around the three different stars, and Fig. 17 shows the corresponding surface UV fluxes. Below $\sim 10^{-3}$ PAL of O_2, the O_3 layers on all three planets become too thin to provide significant UV shielding. In this low-O_2 regime, the high incident UV flux from the F2V star penetrates all the way to the planet's surface, making it an extremely hostile environment for life. The potential for UV damage is quantified in Table 3. We have convolved the surface UV fluxes with action spectra for erythema (skin cancer) (Diffey and McKinlay, 1983) and DNA damage (Van Baalen and O'Donnell, 1972). The latter is shown graphically in Fig. 18. Such action spectra describe the relative effectiveness of different wavelengths in inducing damage. In Table 3 we have normalized the results to a dose rate of unity for Earth at 1 PAL of O_2. For high-O_2 levels the atmospheres of K2V and F2V planets provide better protection from UV damage than does Earth's atmosphere. At low O_2 levels, however, the F2V planet is by far the most dangerous from a UV radiation standpoint. None of the planets looks suitable for surface life at O_2 concentrations $<10^{-2}$ PAL, and even at that O_2 level the dose rate for DNA damage can be 10 times that of modern Earth (although the F2V planet remains surprisingly well protected). When combined with the shorter main sequence lifetimes of such stars—about 3.6 billion years for an F2V star—this suggests that planets orbiting such stars are less likely to be inhabited than planets around G and K stars.

DISCUSSION

Model limitations

We acknowledge certain limitations in our model. The *k*-coefficients used in the IR radiative transfer code (from Mlawer *et al.*, 1997) were derived for temperatures within 30 K of their listed values in the 1976 U.S. Standard Atmosphere. Our calculated upper stratospheric temperatures are routinely lower than this at low O_2 levels. We

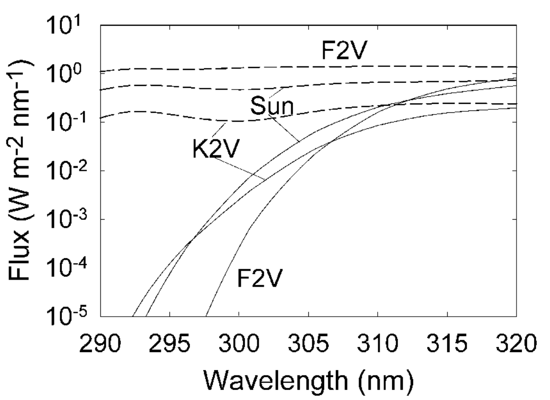

FIG. 15. Incident (dashed curve) and surface (solid curve) UV fluxes for Earth-like planets with 1 PAL O_2 atmospheres circling different types of stars. Fluxes have not been diurnally averaged.

TABLE 2. INCOMING AND GROUND UV FLUXES FOR PLANETS WITH DIFFFERENT O_2 LEVELS AND AROUND DIFFERENT STARS

	Total incoming UV flux (W m^{-2})			
Star	200–400 nm	UV-C (<280 nm)	UV-B (280–315 nm)	UV-A (315–400 nm)
Sun	105.215	6.952	16.087	86.009
K2V	41.824	1.484	4.416	37.229
F2V	221.180	44.044	40.473	146.264
	Total ground UV flux (W m^{-2}) for different O_2 levels			
	200–400 nm	UV-C (<280 nm)	UV-B (280–315 nm)	UV-A (315–400 nm)
Sun				
1 PAL	89.890	10^{-23}	1.335	88.555
10^{-1} PAL	90.176	1.6×10^{-7}	1.657	88.519
10^{-2} PAL	93.386	7.1×10^{-4}	3.452	89.933
10^{-3} PAL	99.419	3.8×10^{-2}	8.162	91.218
10^{-4} PAL	108.521	2.664	14.284	91.574
10^{-5} PAL	110.856	4.351	14.924	91.581
K2V				
1 PAL	39.895	10^{-23}	0.573	39.322
10^{-1} PAL	40.154	9.6×10^{-8}	0.817	39.337
10^{-2} PAL	41.146	2.3×10^{-4}	1.449	39.697
10^{-3} PAL	43.122	0.032	3.025	40.066
10^{-4} PAL	44.494	0.475	3.898	40.122
10^{-5} PAL	45.067	0.847	4.096	40.125
F2V				
1 PAL	144.950	10^{-26}	0.913	144.037
10^{-1} PAL	145.244	4.5×10^{-8}	1.139	144.105
10^{-2} PAL	149.380	3.1×10^{-4}	2.510	146.869
10^{-3} PAL	162.571	0.121	10.497	151.953
10^{-4} PAL	208.422	18.209	36.029	154.184
10^{-5} PAL	216.694	25.187	37.328	154.179

have already noted earlier that the (four-term) *k*-coefficients for absorption of near-IR radiation by CO_2 and H_2O provide a relatively crude estimate of solar heating at low O_2 levels. At O_2 levels above 10^{-3} PAL, the errors resulting from this approximation are minimal because most of the solar heating is produced by absorption of UV radiation by ozone.

The lack of clouds in our model affects our results in two ways: First, our calculated surface temperatures at lower O_2 levels do not include the effects of cloud feedback. This is a minor difficulty at most, as surface temperatures always remain within a few degrees of 288 K. Clouds could have a much bigger effect on our calculated spectra, however. In particular, the 9.6-μm O_3 band can be virtually "washed out" by the presence of widespread, high, cold cirrus clouds (Des Marais *et al.*, 2002). The effect of clouds is best studied by looking at disk-averaged IR spectra of Earth, such as the one obtained by the Mars Observer (Pearl and Christensen, 1997; Seager, 2000).

An important aspect of the photochemical model that has not been discussed is the vertical eddy diffusion profile. The profile used in the model is an empirical one derived by fitting observations of species such as CH_4 and N_2O (Massie and Hunten, 1981). Treating vertical transport as "diffusion" is an approximation to begin with because such transport occurs by both large-scale atmospheric motions (winds) and small-scale turbulence. Without doing an elaborate dynamical calculation, it is thus impossible to estimate how eddy diffusion coefficients should change at lower O_2 levels. However, one can guess that as the stratospheric temperature bulge disappears, the lower stratosphere would become less stable, and vertical diffusion coefficients would increase. To see how much effect this would have on our results, we created a test eddy diffusion profile with three times higher coefficients in the stratosphere for G2V planets at O_2 levels of 10^{-5}–10^{-1} PAL. The amount of water in the stratosphere varies little for 10^{-1}–10^{-3} PAL of

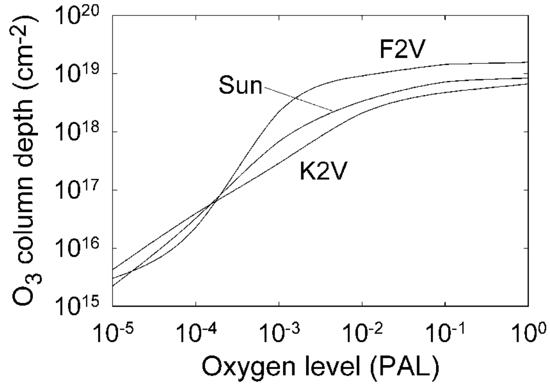

FIG. 16. O_3 column depth as a function of atmospheric O_2 level for planets circling different types of stars.

O_2, but is up to 10 times larger at lower O_2 levels. The effect on ozone is to decrease the peak number density (by 15% at 10^{-1} PAL of O_2 and 22% at 10^{-2} PAL of O_2) and to increase the number densities above and below the peak (by as much as a factor of 2 in the lower stratosphere at 10^{-1} PAL of O_2). The total column depth increases by a much smaller amount, about 6% at 10^{-1} PAL of O_2 and 10% at 10^{-2} PAL of O_2. Changes in column depth at lower O_2 levels are 4% or smaller. Thus, we expect that plausible increases in vertical mixing rates would produce modest, but measurable, effects on the calculated emission spectrum around 9.6 μm, along with small decreases in the flux of UV radiation at the surface. The changes are not so great, however, as to alter our overall conclusions.

Which of these atmospheres might actually exist?

We have performed simulations of a variety of different Earth-like atmospheres. It is appropriate to step back for a moment and consider which of these atmospheres might actually exist on some planet around another star. We should also say a few words about types of Earth-like atmospheres that might exist on extrasolar planets but that have not been considered here.

Let us begin with the latter question. All of the atmospheres modeled here contain appreciable amounts of O_2. By "appreciable," we mean that the O_2 concentrations are much higher than those thought to have existed on early Earth. Recently obtained data on mass-independently fractionated sulfur isotopes in ancient rocks demonstrate that O_2 levels during the Archean and early Paleoproterozoic (3.8–2.3 Ga) were well below 10^{-5} PAL (Farquhar *et al.*, 2000, 2001; Pavlov and Kasting, 2002). CH_4 concentrations in such low-O_2 "Archean" atmospheres are predicted to have been of the order of 1,000 ppm (Catling *et al.*, 2001; Pavlov *et al.*, 2001) and should be observable in both the visible/near-IR and the thermal-IR spectral regions (Schindler and Kasting, 2000; Des Marais *et al.*, 2002). Trace amounts of O_2 and O_3 should have existed in the upper atmosphere as a consequence of atmospheric photochemistry initiated by CO_2 photolysis (see, e.g., Kasting, 1993), but their concentrations should have been too low to be observed remotely (Schindler and Kasting, 2000). Some of the abiotic models discussed by Selsis *et al.* (2002) (particularly their Case B) did indeed have measurable concentrations of both O_2 and O_3, but these models ignored volcanic outgassing of reduced gases and reactions of O_2 with reduced surface minerals. Furthermore, their models were not based on a bal-

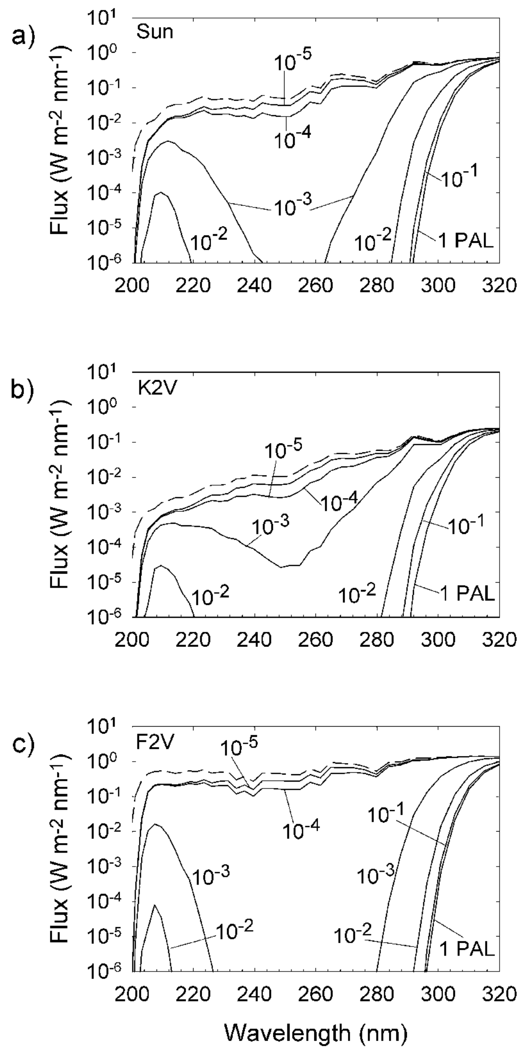

FIG. 17. Incident (dashed curve) and surface (solid curve) UV fluxes at different atmospheric O_2 levels: (a) Earth (Sun), (b) K2V planet, and (c) F2V planet.

TABLE 3. NORMALIZED SURFACE UV DOSE RATES RELATIVE TO PRESENT EARTH FOR ERYTHEMA (SKIN CANCER) AND DNA DAMAGE FOR PLANETS WITH DIFFERENT O_2 LEVELS AND AROUND DIFFERENT STARS

	Oxygen level (PAL)					
Star type	*1*	10^{-1}	10^{-2}	10^{-3}	10^{-4}	10^{-5}
Erythema						
G2V (Sun)	1.00	1.32	4.43	23.57	55.11	60.07
K2V	0.44	0.75	2.27	9.58	13.99	15.33
F2V	0.68	0.82	1.87	18.88	148.87	164.99
DNA						
G2V (Sun)	1.00	1.54	10.44	214.13	3,688.03	5,459.83
K2V	0.50	1.19	8.39	173.29	813.07	1,236.71
F2V	0.38	0.51	1.85	63.72	16,316.62	22,651.23

anced atmospheric hydrogen budget (Kasting and Brown, 1998; Kasting and Catling, 2003); hence, they underestimated H_2 concentrations and overestimated O_2 and O_3. A discussion of the upper limits on abiotically generated O_2 can be found in Kasting (1997) and Des Marais *et al.* (2002). Selsis *et al.* (2002) did point out a possible interference problem between the O_3 9.6-μm band and the 9.4-μm and 10.4-μm CO_2 "hot" bands that could make detection of O_3 problematical in high-CO_2, high-O_2 atmospheres. Note that all of the atmospheres studied here assumed modern-Earth CO_2 concentrations, so this overlap problem was not encountered.

The second question is which of the relatively high-O_2 atmospheres examined here might actually have existed. Although we have performed calculations down to 10^{-5} PAL of O_2, we do not think that Earth's atmosphere could have been stable for any appreciable length of time at O_2 levels between 10^{-5} PAL and ~10^{-2} PAL. The reason has to do with the geochemical cycles that control the O_2 concentration. In the low-O_2, "Archean" atmospheres just discussed, the net rate of O_2 production from photosynthesis followed by organic carbon burial in sediments must have been lower than half the rate at which H_2 was produced by volcanism and rainout of oxidized gases (Walker, 1977; Kasting and Brown, 1998). (The factor of one-half results from the stoichiometry of the reaction: $2\ H_2 + O_2 \rightarrow 2\ H_2O$.) That is what kept the Archean atmosphere low in O_2. Once the balance shifted (apparently at ~2.3 Ga) so that net production of O_2 exceeded half the H_2 production rate, O_2 should have accumulated in the atmosphere until it was high enough to oxidize reduced materials (Fe^{2+}, S^{2-}, and C^0) in rocks during weathering. It is difficult to determine a quantitative relationship between O_2 levels and oxidative weathering rates, but O_2 concentrations exceeding 10^{-2} PAL are almost certainly required (Holland, 1984, 2003; Lasaga and Ohmoto, 2002; Ohmoto, 2003). As we have discussed above, Mid-Proterozoic O_2 levels are

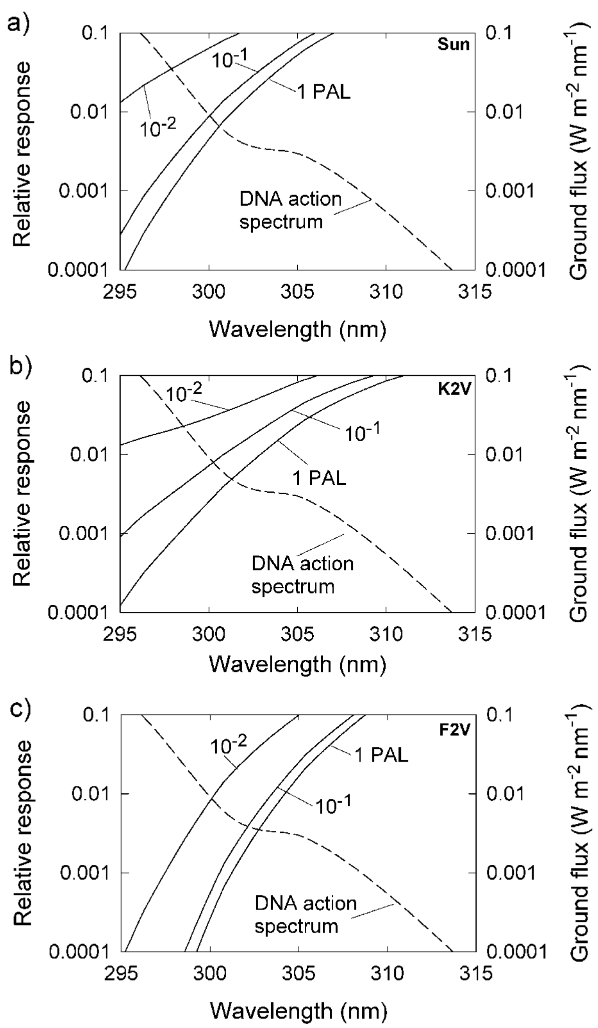

FIG. 18. Surface UV flux (solid curves) and DNA action spectra (dashed curves) at different atmospheric O_2 levels: (a) Earth (Sun), (b) K2V planet, and (c) F2V planet.

thought to have been in the range of 10^{-2} PAL to a few times 10^{-1} PAL. This is a particularly interesting range of O_2 concentrations because CH_4 and O_2 might both have been detectable remotely during this time.

CONCLUSIONS

We have presented simulated atmospheric compositions and visible/near-IR and thermal-IR spectra for Earth-like planets containing 10^{-5}–1 PAL of O_2 in their atmospheres and orbiting G2V, F2V, and K2V stars. O_2 is potentially observable in the visible (0.76 μm) down to $\sim 10^{-2}$ PAL of O_2 for planets circling all three types of stars. O_3 is observable in the thermal IR (9.6 μm) down to at least 10^{-3} PAL of O_2 and perhaps even lower for the planet around the F2V star. At 1 PAL of O_2, the ozone band around the F2V star is weaker than that around the Sun or the K2V star because of the relatively high stratospheric temperature.

We have also computed surface UV fluxes and relative dose rates for erythema and DNA damage for these simulated atmospheres. Planets around K2V and F2V stars both exhibit better UV protection than does Earth at an O_2 level of 1 PAL. Thus, advanced life (including humans) could conceivably survive in both environments. Surface UV fluxes increase dramatically for O_2 levels below 10^{-2} PAL, with the planet around the F2V star exhibiting the highest increases because of the high intrinsic UV luminosity of the star. The high surface UV fluxes on low-O_2 planets circling F stars could pose a significant threat to biological evolution. An O_2 level of 10^{-2} PAL should have been reached on Earth soon after the initial rise of O_2 at 2.3 Ga, so Earth's biota have been well protected from UV radiation since that time.

Perhaps the most interesting result of our modeling is the prediction that O_2 (or O_3) and CH_4 might be simultaneously observed at thermal-IR wavelengths in "Mid-Proterozoic-type" atmospheres containing modest amounts ($\sim$0.1 PAL) of O_2 and perhaps tens of parts per million of CH_4. Such an observation would be even firmer evidence of extraterrestrial life than the observation of a high-O_2 planet like modern Earth. Simultaneous detection of O_2 and CH_4 at visible/near-IR wavelengths would be much more difficult. Thus, there could be a slight scientific preference for doing the TPF mission in the thermal IR.

ACKNOWLEDGMENTS

This material is based upon work supported by the National Aeronautics and Space Administration through the NASA Astrobiology Institute under Cooperative Agreements CAN-97-OSS-01 and CAN-00-OSS-01 issued through the Office of Space Science. M.C. thanks NASA for supporting his participation in this study through contract 1234394 between the Jet Propulsion Laboratory and the University of California Berkeley, under the NASA Astrobiology Institute's "Virtual Planetary Laboratory" project.

ABBREVIATIONS

LW, longwave; IUE, International Ultraviolet Explorer; PAL, present atmospheric level; RRTM, rapid radiative transfer model; SMART, Spectral Mapping Atmospheric Radiative Transfer; SW, shortwave; TPF, Terrestrial Planet Finder.

REFERENCES

Anbar, A.D. and Knoll, A.H. (2002) Proterozoic ocean chemistry and evolution: a bioinorganic bridge? *Science* 297, 1137–1142.

Beichman, C.A., Woolf, N.J., and Lindensmith, C.A. (1999) *The Terrestrial Planet Finder (TPF): A NASA Origins Program to Search for Habitable Planets*, JPL Publication 99–3, NASA Jet Propulsion Laboratory, Pasadena, CA.

Burnashev, V.I. (1985) Catalogue of the energy distribution data in spectra of stars in the uniform spectrophotometric system. *Abastumanskaya Astrofiz. Obs. Bull.* 59, 83–89.

Buser, R. and Kurucz, R.L. (1992) A library of theoretical stellar flux spectra. I—Synthetic UBVRI photometry and the metallicity scale for F- to K-type stars. *Astron. Astrophys.* 264, 557–591.

Canfield, D.E. (1998) A new model for Proterozoic ocean chemistry. *Nature* 396, 450–453.

Canfield, D.E., Habicht, K.S., and Thamdrup, B. (2000) The Archean sulfur cycle and the early history of atmospheric oxygen. *Science* 288, 658–661.

Catling, D.C., Zahnle, K.J., and McKay, C.P. (2001) Biogenic methane, hydrogen escape, and the irreversible oxidation of early Earth. *Science* 293, 839–843.

Cayrel de Strobel, G., Hauck, B., Francois, P., Thevenin, F., Friel, E., Mermilliod, M., and Borde, S. (1992) A catalogue of Fe/H determinations—1991 edition. *Astron. Astrophys. Suppl. Ser.* 95, 273–336.

Cohen, M., Megeath, T.G., Hammersley, P.L., Martin-Luis, F., and Stauffer, J. (2003) Spectral irradiance calibration in the infrared. XIII. "Supertemplates" and onorbit calibrators for the SIRTF Infrared Array Camera. *Astron. J.* 125, 2645–2663.

Cumming, A., Marcy, G.W., and Butler, R.P. (1999). The Lick planet search: detectability and mass thresholds. *Astrophys. J.* 526, 890–915.

Des Marais, D.J., Harwit, M.O., Jucks, K.W., Kasting, J.F., Lin, D.N.C., Lunine, J.I., Schneider, J., Seager, S., Traub, W.A., and Woolf, N.J. (2002) Remote sensing of planetary properties and biosignatures on extrasolar terrestrial planets. *Astrobiology* 2, 153–181.

Diffey, B.L. and McKinlay, A.F. (1983) The UVB content of the 'UVA fluorescent lamps' and its erythemal effectiveness in human skin. *Phys. Med. Biol.* 28, 351–358.

Farquhar, J., Bao, H., and Thiemans, M. (2000) Atmospheric influence of Earth's earliest sulfur cycle. *Science* 289, 756–758.

Farquhar, J., Savarino, J., Airieau, S., and Thiemens, M.H. (2001) Observation of wavelength-sensitive mass-independent sulfur isotope effects during SO_2 photolysis: application to the early atmosphere. *J. Geophys. Res.* 106, 1–11.

Habing, H.J., Dominik, C., Jourdain de Muizon, M., Laureijs, R.J., Kessler, M.F., Leech, K., Metcalfe, L., Salama, A., Siebenmorgen, R., Trams, N., and Bouchet, P. (2001) Incidence and survival of remnant disks around main-sequence stars. *Astron. Astrophys.* 365, 545–561.

Holland, H.D. (1984) *The Chemical Evolution of the Atmosphere and Oceans*, Princeton University Press, Princeton, NJ.

Holland, H.D. (2003) Discussion of the article by A.C. Lasaga and H. Ohmoto on "The oxygen geochemical cycle: dynamics and stability," *Geochim. Cosmochim. Acta* 66, 361–381, 2002. *Geochim. Cosmochim. Acta* 67, 787–789.

Houghton, J.T., Meira Filho, L.G., Bruce, J., Lee, H., Callander, B.A., Haites, E., Harris, N., and Maskel, K. (1994) *Climate Change, 1994: Radiative Forcing of Climate Change and an Evaluation of the IPCC IS92 Emission Scenarios*, Cambridge University Press, Cambridge, UK.

Kasting, J.F. (1993) Earth's early atmosphere. *Science* 259, 920–926.

Kasting, J.F. (1997) Habitable zones around low mass stars and the search for extraterrestrial life. *Origins Life* 27, 291–307.

Kasting, J.F. and Ackerman, T.P. (1986) Climatic consequences of very high CO_2 levels in the earth's early atmosphere. *Science* 234, 1383–1385.

Kasting, J.F. and Brown, L.L. (1998) Setting the stage: the early atmosphere as a source of biogenic compounds. In *The Molecular Origins of Life: Assembling the Pieces of the Puzzle*, edited by A. Brack, Cambridge University Press, New York, pp. 35–56.

Kasting, J.F. and Catling, D. (2003) Evolution of a habitable planet. *Annu. Rev. Astron. Astrophys.* 41, 429–463.

Kasting, J.F. and Donahue, T.M. (1980) The evolution of atmospheric ozone. *J. Geophys. Res.* 85, 3255–3263.

Kasting, J.F., Holland, H.D., and Pinto, J.P. (1985) Oxidant abundances in rainwater and the evolution of atmospheric oxygen. *J. Geophys. Res.* 90, 10497–10510.

Kasting, J.F., Whitmire, D.P., and Reynolds, R.T. (1993) Habitable zones around main sequence stars. *Icarus* 101, 108–128.

Kasting, J.F., Whittet, D.C.B., and Sheldon, W.R. (1997) Ultraviolet radiation from F and K stars and implications for planetary habitability. *Orig. Life Evol. Biosph.* 27, 413–420.

Kurucz, R.L. (1979) Model atmospheres for G, F, A, B, and O stars. *Astrophys. J. Suppl. Ser.* 1–340.

Lasaga, A.C. and Ohmoto, H. (2002) The oxygen geochemical cycle: dynamics and stability. *Geochim. Cosmochim. Acta* 66, 361–381.

Léger A. (2000) Strategies for remote detection of life: Darwin-IRSI and TPF missions. Adv. *Space Res.* 25, 2209–2223.

Léger, A., Pirre, M., and Marceau, F.J. (1993) Search for primitive life on a distant planet: relevance of O_2 and O_3 dectections. *Astron. Astrophys.* 277, 309–313.

Levine, J.S., Hays, P.B., and Walker, J.C.G. (1979) The evolution and variability of atmospheric ozone over geologic time. *Icarus* 39, 295–309.

Lovelock, J.E. (1965) A physical basis for life detection experiments. *Nature* 207, 568–570.

Manabe, S. and Wetherald, R.T. (1967) Thermal equilibrium of the atmosphere with a given distribution of relative humidity. *J. Atmos. Sci.* 24, 241–259.

Massa, D. and Fitzpatrick, E. L. (2000) A recalibration of IUE NEWSIPS low-dispersion data *Astrophys. J. Suppl. Ser.* 126, 517–535.

Massa, D., Van Steenberg, M.E., Oliversen, N., and Lawton, P. (1998) Science verification of the IUE Final Archive Data Products. In *Special Publication 413: UV Astrophysics Beyond the IUE Final Archive*, edited by W. Wamsteker and R. Gonzalez Riestra, ESA Publications Division, Noordwijk, The Netherlands, pp. 723–726.

Massie, S.T. and Hunten, D.M. (1981) Stratospheric eddy diffusion coefficients from tracer data. *J. Geophys. Res.* 86, 9859–9868.

McClatchey, R.A., Fenn, R.W., Selby, J.E.A., Volz, F.E., and Garing, J.S. (1971) *Technical Report ASCRL-72-0279*, Air Force Cambridge Research Laboratory, Bedford, MA.

Meadows, V.S. and Crisp, D. (1996) Ground-based near-infrared observations of the Venus nightside: the thermal structure and water abundance near the surface. *J. Geophys. Res.* 101(E2), 4595–4622.

Mlawer, E.J., Taubman, S.J., Brown, P.D., Iacono, M.J., and Clough, S.A. (1997) Radiative transfer for inhomogeneous atmospheres: RRTM, a validated correlated-*k* model of the longwave. *J. Geophys. Res.* 102, 16663–16682.

Ohmoto, H. (2003) Reply to comments by H.D. Holland on "The oxygen geochemical cycle: dynamics and stability," *Geochim. Cosmochim. Acta* 66, 361–381, 2002. *Geochim. Cosmochim. Acta* 67, 791–795.

Owen, T. (1980) The search for early forms of life in other planetary systems: future possibilities afforded by spectroscopic techniques. In *Strategies for Search for Life in the Universe*, edited by M.D. Papagiannis, Reidel, Dordrecht, The Netherlands, pp. 177–185.

Pavlov, A.A. and Kasting, J.F. (2002) Mass-independent fractionation of sulfur isotopes in Archean sediments:

strong evidence for an anoxic Archean atmosphere. *Astrobiology* 2, 27–41.

Pavlov, A.A., Kasting, J.F., Brown, L.L., Rages, K.A., and Freedman, R. (2000) Greenhouse warming by CH_4 in the atmosphere of early Earth. *J. Geophys. Res.* 105, 11981–11990.

Pavlov, A.A., Kasting, J.F., and Brown, L.L. (2001) UV-shielding of NH_3 and O_2 by organic hazes in the Archean atmosphere. *J. Geophys. Res.* 106, 23267–23287.

Pavlov, A.A., Hurtgen, M.T., Kasting, J. F., and Arthur, M.A. (2003) Methane-rich Proterozoic atmosphere? *Geology* 31, 87–90.

Pearl, J.C. and Christensen, P.R. (1997) Initial data from the Mars Global Surveyor thermal emission spectrometer experiment: observations of the Earth. *J. Geophys. Res.* 102, 10875–10880.

Ratner, M.I. and Walker, J.C.G. (1972) Atmospheric ozone and the history of life. *J. Atmos. Sci.* 29, 803–808.

Sagan, C., Thompson, W.R., Carlson, R., Gurnett, D., and Hord, C.A. (1993) Search for life on Earth from the Galileo spacecraft. *Nature* 365, 715–721.

Schindler, T.L. and Kasting, J.F. (2000) Synthetic spectra of simulated terrestrial atmospheres containing possible biomarker gases. *Icarus* 145, 262–271.

Seager, S. (2000) The search for Earth-like extrasolar planets. *Earth Planet. Sci. Lett.* 160, 1–10.

Selsis, F., Despois, D., and Parisot, J.-P. (2002) Signature of life on exoplanets: can Darwin produce false positive detections? *Astron. Astrophys.* 388, 985–1003.

Stamnes, K., Tsay, S.-C., Jayaweera, K., and Wiscombe, W. (1988) Numerically stable algorithm for discrete-ordinate-method radiative transfer in multiple scattering and emitting layered media. *Appl. Opt.* 27, 2502–2509.

Toon, O.B., McKay, C.P., Ackerman, T.P., and Santhanam, K. (1989) Rapid calculation of radiative heating rates and photodissociation rates in inhomogeneous multiple scattering atmospheres. *J. Geophys. Res.* 94, 16287–16301.

Van Baalen, C. and O'Donnell, R. (1972) Action spectra for ultraviolet killing and photoreactivation in the blue-green alga *Agmenellum quadruplicatum. Photochem. Photobiol.* 15, 269–274.

Walker, J.C.G. (1977) *Evolution of the Atmosphere*, Macmillan, New York.

Address reprint requests to:
Dr. Antígona Segura
443 Deike Building
University Park
State College, PA 16803

E-mail: antigona@essc.psu.edu